VIP Heterogeneous Catalysis

DOI: 10.1002/ange.201300276

Monodisperse AgPd Alloy Nanoparticles and Their Superior Catalysis for the Dehydrogenation of Formic Acid**

Sen Zhang, Önder Metin, Dong Su, and Shouheng Sun**

Formic acid (FA, HCOOH) is a common small organic acid with a melting point of 8.4 °C and boiling point of 100.8 °C. It can undergo a dehydrogenation reaction, $HCOOH \rightarrow H_2 + CO_2$, releasing H_2 that will be important for hydrogen-based energy applications.[1] Traditionally, the dehydrogenation of FA is catalyzed by metal complexes dissolved in an organic solvent and the catalysis is enhanced by adding an additive, such as sodium formate or amine adducts.[2] To make more practical catalyst for the dehydrogenation reaction of FA, heterogeneous catalysts based on metal nanoparticles (NPs) have been developed. These catalysts are generally more stable but much less active than the homogeneous ones.[3] Recently, bimetallic NP catalysts were found to be more active than their single component counterparts for the dehydrogenation of FA.[4] For example, AgPd NPs supported on cerium oxide or AuPd NPs immobilized in a metal–organic framework showed an enhanced FA dehydrogenation catalysis with the initial turnover frequency (TOF) reaching 210 h^{-1} or 192 h^{-1} at 90 °C, respectively.[5] However, the high rate of hydrogen generation observed from these heterogeneous catalysts could only be achieved when an additive was present and the reaction was maintained at temperatures close to 100 °C.[6] Under these "harsh" conditions, HCOOH was also subject to an undesired dehydration reaction, $HCOOH \rightarrow H_2O + CO$.[7] Interestingly, Ag/Pd core/shell NPs were found to be promising in catalyzing the dehydrogenation of FA in an aqueous FA solution at lower temperatures (up to 50 °C) without any additive.[8] But their initial TOFs were in the range of 125–252 h^{-1} at temperatures between 25–50 °C.

Considering the limitation seen from the previous syntheses in controlling the NP size and composition, we decided to re-evaluate the binary alloy NPs on their catalysis for the dehydrogenation of FA. Our very recent report showed that monodisperse 4 nm AuPd NPs were more active in catalyzing the dehydrogenation of FA in water at 50 °C without using any additive and their initial TOF reached 230 h^{-1}.[9] Encouraged by this result, we further improved our solution phase synthesis and produced monodisperse 2.2 nm AgPd NPs with the desired composition controls. We found that these monodisperse 2.2 nm AgPd alloy NPs were a highly active heterogeneous catalyst for the dehydrogenation of FA. In water without any additive, the $Ag_{42}Pd_{58}$ NPs showed the highest catalytic activity among all AgPd NPs tested with their initial TOF reaching 382 h^{-1} at 50 °C and apparent activation energy at 22 ± 1 kJ mol^{-1}. These are the best values ever reported by a heterogeneous catalyst for the dehydrogenation of FA in aqueous solution. It demonstrates the great potential of binary alloy NPs as a more practical catalyst for the dehydrogenation of FA and hydrogen generation.

The 2.2 nm AgPd alloy NPs were synthesized by co-reduction of silver(I) acetate, Ag(Ac), and palladium(II) acetylacetonate, $Pd(acac)_2$, in oleylamine (OAm), oleic acid (OA) and 1-octadecene (ODE) at 180 °C (Experimental Section). Here, OA served as a surfactant and OAm was added both as a co-surfactant and mild reducing agent. The composition of the AgPd NPs ($Ag_{25}Pd_{75}$, $Ag_{42}Pd_{58}$, $Ag_{52}Pd_{48}$, $Ag_{60}Pd_{40}$, and $Ag_{80}Pd_{20}$) were controlled by varying the molar ratio of $Ag(Ac)/Pd(acac)_2$ and analyzed by inductively coupled plasma-atomic emission spectroscopy (ICP-AES; Table S1 in the Supporting Information). Transmission electron microscopy (TEM) images of the as-synthesized AgPd NPs show that they have a mean particle size of 2.2 ± 0.1 nm (Figure 1 A and Figure S1A–D). Under similar reaction conditions, we also synthesized 2.2 ± 0.1 nm Ag NPs (Figure S1E) and 4.5 ± 0.2 nm Pd NPs (Figure S1F) by reducing only Ag(Ac) or $Pd(acac)_2$. Different from the previous approaches to AgPd alloy NPs (larger than 7 nm) by a strong reducing agent,[5a] or a multi-step reaction scheme (diffusing Pd into Ag seeds at a high temperature),[10] our one-step co-reduction of metal salts by OAm is highly efficient in producing monodisperse AgPd NPs at a particle size of only 2.2 nm. The use of an excess amount of OA was crucial for controlling the NP size. If OA was present in a small amount (e.g. 0.5 mL) or no OA was used, polydisperse AgPd NPs were obtained (Figure S2A&B).

A representative high-resolution (HR) TEM image of the 2.2 nm $Ag_{42}Pd_{58}$ NPs (Figure 1 B) shows the (111) lattice fringe distance of 0.23 nm, which is between the (111) lattice spacing of face-centered cubic (*fcc*) Ag (0.24 nm) and *fcc* Pd

[*] S. Zhang, Dr. Ö. Metin, Dr. S. Sun
Department of Chemistry, Brown University
Providence, RI 02912 (USA)
E-mail: ssun@brown.edu
Dr. Ö. Metin
Department of Chemistry, Faculty of Science
Atatürk University, 25240 Erzurum (Turkey)
E-mail: ometin@atauni.edu.tr
Dr. D. Su
Brookhaven National Laboratory
Center for Functional Nanomaterials
Upton, NY 11973-5000 (USA)

[**] This work was supported by the U.S. Army Research Laboratory and the U.S. Army Research Office under the Multi University Research Initiative (MURI, grant number W911NF-11-1-0353) on "Stress-Controlled Catalysis via Engineered Nanostructures". Partial work carried out at the Center for Functional Nanomaterials, Brookhaven National Laboratory, was supported by the U.S. Department of Energy, Office of Basic Energy Sciences, under contract number DE-AC02-98CH10886.

Supporting information for this article is available on the WWW under http://dx.doi.org/10.1002/anie.201300276.

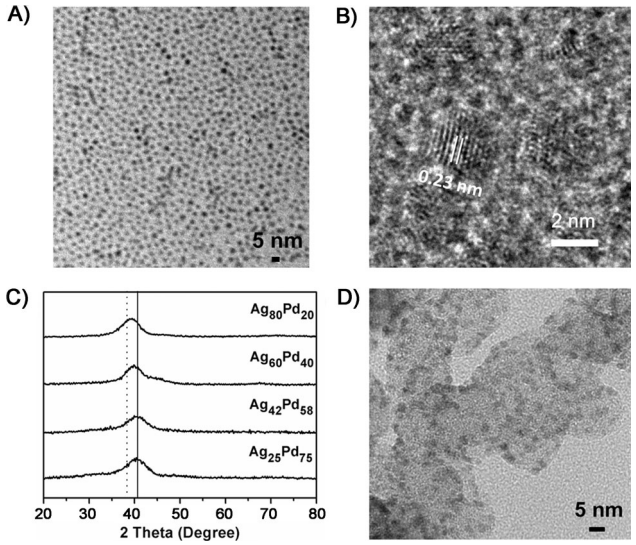

Figure 1. A) TEM image of the 2.2 nm $Ag_{42}Pd_{58}$ NPs. B) HRTEM image of the 2.2 nm $Ag_{42}Pd_{58}$ NPs. C) XRD patterns of the 2.2 nm $Ag_{25}Pd_{75}$, $Ag_{42}Pd_{58}$, $Ag_{60}Pd_{40}$ and $Ag_{80}Pd_{20}$ NPs (dashed line and solid line denote standard (111) peak positions of bulk Ag and Pd, respectively). D) TEM image of the carbon-supported 2.2 nm $Ag_{42}Pd_{58}$ NPs after treatment with acetic acid.

(0.22 nm) NPs. Figure 1 C is the X-ray diffraction (XRD) patterns of the 2.2 nm AgPd NPs. The AgPd NPs have a very weak peak intensity because of their small size. With the Ag amount increased in AgPd, the (111) peak shifts to a lower angle towards Ag(111) because of the increase of the lattice parameters, indicating that AgPd is formed as an alloy and not as a core/shell structure. Furthermore, AgPd NPs show almost no surface plasmon resonance (SPR) absorption in the UV/Vis spectra, whereas Ag NPs have a very strong SPR absorption at 425 nm (Figure S3). This SPR "quenching" caused by the alloying effect was also observed in other Ag- and Au-based alloy NPs.[11]

To study NP catalysis for the dehydrogenation of FA in water, we deposited Ag, Pd, or AgPd NPs on Ketjen carbon (C) and cleaned these C-NPs by acetic acid treatment and ethanol washing followed by drying under vacuum (Experimental Section). The representative TEM image (Figure 1 D) and the relevant ICP-AES analysis (Table S2) revealed that these C-AgPd NPs preserved their size, morphology, and composition after the cleaning process. The metal contents of the C-AgPd, C-Pd, and C-Ag catalysts were measured (by ICP-AES) to have 17 wt % AgPd, 19 wt % Pd, and 18 wt % Ag, respectively. The catalytic activity of the C NP catalysts in the dehydrogenation of FA was evaluated in a gas burette system. Figure 2 A shows the plots of volume of gas ($CO_2 + H_2$) generated versus the reaction time during the dehydrogenation of the aqueous FA solution (10 mL, 1 M FA solution at 50 °C) catalyzed by different C-AgPd and C-Pd catalysts. We can see that most C-AgPd catalysts have a higher activity than the C-Pd NPs, except for C-$Ag_{80}Pd_{20}$. The C-$Ag_{25}Pd_{75}$, C-$Ag_{42}Pd_{58}$, and C-$Ag_{52}Pd_{48}$ catalysts have the initial TOF of 318, 382, and 228 h^{-1}, respectively. They are even more active than the state-of-the-art AgPd alloy (TOF = 210 h^{-1} at 92 °C) and Ag/Pd core/shell NPs (TOF = 252 h^{-1} at 50 °C). Figure 2 B shows the plot of TOF versus the mole fraction of Ag for the C-AgPd catalyst at different compositions. The TOF increases with increasing Ag mole ratio up to 0.42 and then decreases. The observed "volcano"-type activity of the C-AgPd catalyst versus the Ag/Pd composition indicates that although neither Ag nor Pd is active for catalyzing the dehydrogenation reaction of FA, alloying Ag with Pd provides a necessary synergistic effect on the catalysis and $Ag_{42}Pd_{58}$ is the optimum catalyst for catalyzing the dehydrogenation of FA. This further supports that Ag and Pd form a uniform alloy structure in the synthesis.

Since dehydration route of FA ($HCOOH \rightarrow CO + H_2O$) is generally associated with the dehydrogenation at relatively high reaction temperatures ($T > 60$ °C),[3,7] we also tested our reaction and characterized the evolving gas mixture with FT-IR and mass spectroscopy. We found no detectable amount of CO in the gas mixture generated from the C-$Ag_{42}Pd_{58}$ catalyzed the dehydrogenation of FA (Figure S4). After reacting the gas mixture with the aqueous NaOH solution, the volumes of CO_2 and H_2 were estimated and the gas mixture was found to consist of equal molar amounts of CO_2 and H_2 (Figure S5), proving that the AgPd catalyst promotes complete dehydrogenation of FA into CO_2 and H_2. The drastic dehydrogenation activity enhancement of these 2.2 nm AgPd NPs is likely caused by their small size and the synergistic effect between Ag and Pd in the alloy structure that inhibits the adsorption of CO on Pd. This is consistent with what was observed on the CeO_2-supported MPd (M = Ag, Au) systems.[5a] However, our system is also different from the CeO_2-supported MPd catalyst in which the enhanced activity was believed to originate from the NP-support interactions,[5a] and ours seem to show a more drastic alloy effect with their catalysis optimized when the AgPd catalysts has the composition $Ag_{42}Pd_{58}$.

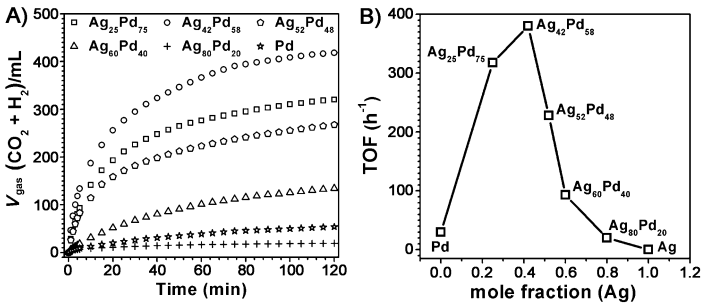

Figure 2. A) The plots of generated gas ($CO_2 + H_2$) versus time during the dehydrogenation of an aqueous FA solution (10 mL of 1 M, 50 °C) in the presence of C-AgPd and C-Pd catalysts and B) TOF vs. mole fraction of Ag for the C-AgPd catalysts at different Ag and Pd compositions.

The concentration of the NP catalyst, FA concentration, and temperature effects were studied to obtain more kinetic information about the dehydrogenation of FA. In the first set of experiments, the dehydrogenation reaction was performed at different catalyst concentrations in the range of 10–40 mg (1.6–6.4 mM) $Ag_{42}Pd_{58}$ by keeping the FA concentration at

1.0 M and the temperature at 50 °C. The volume of generated gas ($CO_2 + H_2$) was plotted versus the reaction time during the dehydrogenation of FA at different catalyst concentrations (Figure S6A). The hydrogen generation rates for each catalyst concentration were calculated from the linear portion of each plot comprising a reaction duration of 20 minutes. Figure S6B shows the logarithmic plot of the hydrogen generation rate versus the AgPd concentration. The line with a slope of 0.88 in Figure S6B indicates that the reaction is close to first-order with respect to the catalyst concentration.

To study FA concentration effect on the gas generation rate, we kept the C-$Ag_{42}Pd_{58}$ concentration at 3.2 mM $Ag_{42}Pd_{58}$ and the temperature at 50 °C. Figure 3A shows the volume of generated gas ($CO_2 + H_2$) versus time at different FA concentrations. The initial TOFs (h^{-1}) were calculated and presented in Figure 3B. From Figure 3A&B, we can see

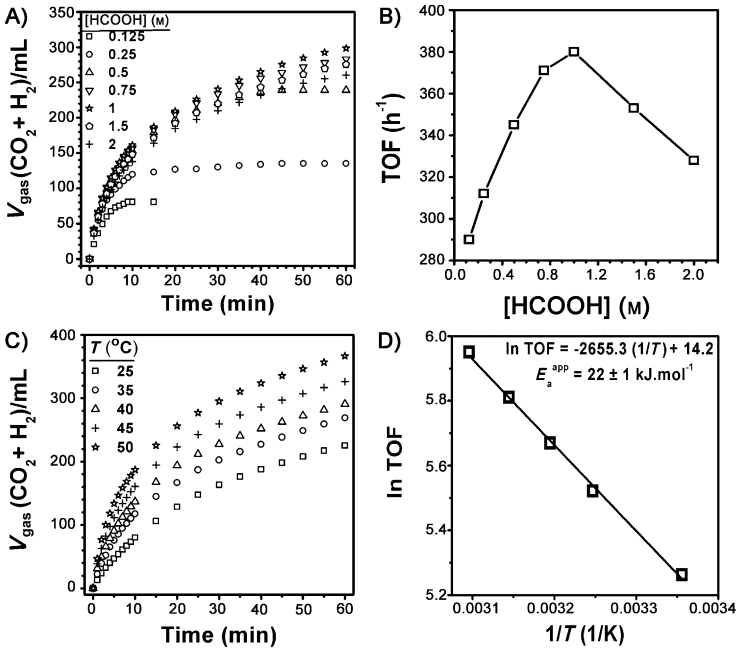

Figure 3. A) The volume of the generated gas ($CO_2 + H_2$) versus time for the dehydrogenation of FA catalyzed by the C-$Ag_{42}Pd_{58}$ at different FA concentrations (0.125–2 M). B) Plot of initial TOF (h^{-1}) versus the FA concentration. C) Volume of the generated gas ($CO_2 + H_2$) versus time for the dehydrogenation of FA catalyzed by C-$Ag_{42}Pd_{58}$ at different different temperatures (25–50 °C). D) Arrhenius plot (ln(TOF) vs. 1/*T*).

a volcano-shaped relationship between TOF and HCOOH concentration. The gas generation rate increases almost linearly with the FA concentration in the range of 0.125–1.0 M, but drops when the HCOOH concentration is higher than 1 M. This, plus the catalyst inactivity observed for the dehydrogenation of pure FA, reveals that a large amount of water plays an indispensable role in the catalytic dehydrogenation of FA. To measure the ease of the dehydrogenation reaction catalyzed by the AgPd alloy catalyst, we recorded the time-dependent H_2 generation at different temperatures (25–50 °C) in the presence of C-$Ag_{42}Pd_{58}$ (3.2 mM AgPd) and FA (1 M), as shown in Figure 3C. By converting the reactivity into TOF and by plotting the logarithmic TOF vs. 1/*T*, we obtained the Arrhenius plot (Figure 3D). From the linear Arrhenius behavior, we calculated the apparent activation energy (E_a^{app}) to be 22 ± 1 kJ mol^{-1} for the C-$Ag_{42}Pd_{58}$ catalyzed the dehydrogenation reaction of FA. This is the lowest value ever reported for the dehydrogenation reaction of FA catalyzed by a heterogeneous catalyst.

We further tested briefly the stability of the C-$Ag_{42}Pd_{58}$ catalyst by performing the dehydrogenation of FA in water at 50 °C and recovering the catalyst from the solution after the reaction completion for the next round of reaction. Our tests showed that the C-$Ag_{42}Pd_{58}$ catalyst preserved 90% of its initial activity after the fourth run (Figure S7A). We analyzed the recovered catalyst by ICP-AES and TEM (Figure S7B). We found no obvious change in the Ag/Pd composition, catalyst loading on carbon, and NP morphology. These findings indicate that the C-$Ag_{42}Pd_{58}$ catalyst was stable under the current FA dehydrogenation condition and could be re-used for multiple rounds of the dehydrogenation reaction.

Herein, we have demonstrated a facile approach to a composition-controlled synthesis of monodisperse 2.2 nm AgPd NPs. These 2.2 nm AgPd NPs are highly active and durable as catalysts for the dehydrogenation of FA and for hydrogen generation without the need of any additive. Under our evaluation condition (in water at 50 °C), the AgPd NPs show the composition-dependent catalysis and the $Ag_{42}Pd_{58}$ NPs have the highest activity with an initial TOF of 382 h^{-1} and an apparent activation energy of 22 ± 1 kJ mol^{-1}—the best catalytic performance ever reported among all heterogeneous catalysts tested for the dehydrogenation of FA in aqueous solution. This, combining with the fact that Pd and Ag NPs are much less active in catalyzing the dehydrogenation of FA, proves the unique approach in using alloying effects to enhance NP catalysis. With the desired control on the NP sizes, compositions, and shapes, NP catalysis for the dehydrogenation of FA can be further optimized and a new type of heterogeneous catalyst may be developed for hydrogen generation and for hydrogen-based energy device applications.

Experimental Section

Synthesis of AgPd NPs: Under a gentle nitrogen flow, 0.084 g of silver(I) acetate (Ag(Ac), 0.5 mmol) and 0.15 g of palladium(II) acetylacetonate ($Pd(acac)_2$, 0.5 mmol) were magnetically stirred in 4.5 mL of oleic acid (OAc), 0.5 mL of oleylamine (OAm), and 10 mL of 1-octadecene (ODE). The mixture was heated to 60 °C to generate a homogeneous solution. Then the solution was heated to 180 °C at a rate of 3–5 °C minutes^{-1} and kept at this temperature for 20 minutes during which the transparent solution gradually turned into brown and finally dark-brown color. Once the reaction solution was cooled down to room temperature, the NPs were separated by adding isopropanol (50 mL) and centrifugation (9500 rpm, 8 minutes). To remove the organic impurities and precursor residues, the product was redispersed in 10 mL of hexane and then recollected by adding 40 mL of ethanol and centrifugation (9500 rpm, 8 minutes). This synthesis yielded $Ag_{42}Pd_{58}$NPs (yield: 95%), which were dispersed in hexane for future use. Under the same

reaction condition, 0.134 g of Ag(Ac) (0.8 mmol) and 0.06 g of $Pd(acac)_2$ (0. 2 mmol) led to the formation of $Ag_{80}Pd_{20}$ NPs; 0. 126 g of Ag(Ac) (0.75 mmol) and 0.075 g of $Pd(acac)_2$ (0. 25 mmol) generated $Ag_{60}Pd_{40}$ NPs; 0. 1 g of Ag(Ac) (0.6 mmol) and 0.12 g of $Pd(acac)_2$ (0. 4 mmol) produced $Ag_{52}Pd_{48}$ NPs; 0. 042 g of Ag(Ac) (0.25 mmol) and 0.225 g of $Pd(acac)_2$ (0. 75 mmol) yielded $Ag_{25}Pd_{75}$ NPs. Under similar conditions, 0.168 g of Ag(Ac) (1 mmol) in the absence of $Pd(acac)_2$ yielded 2.2 nm Ag NPs. The synthesis of 4.5 nm Pd NPs was conducted according to a protocol published elsewhere.[12]

Preparation of C-NP catalysts: In 10 mL of hexane 50 mg of Ketjen carbon were suspended and sonicated for 15 minutes. Next, about 25 mg of NPs in hexane was added dropwise into the carbon support mixture under sonication. The resulted mixture was sonicated for 1 h to ensure NP adsorption onto the carbon support. The C-NPs were separated by centrifugation and washed with ethanol. Next, the C-NPs were suspended in 30 mL of acetic acid and the suspension was heated for 10 h at 70 °C. 30 mL of ethanol was added and the mixture was centrifuged at 8500 rpm for 6 minutes. This ethanol washing procedure was repeated three times. The C-NPs were recovered and dried under vacuum.

Formic acid dehydrogenation: In 9.6 mL of water 20 mg of C-NP catalysts were dispersed by sonication and then 0.4 mL of formic acid was injected into the catalyst solution at 50 °C. The volume of the gas ($CO_2 + H_2$) generated during the catalytic reaction was monitored by a gas burette system.

Received: January 11, 2013
Published online: February 20, 2013

Keywords: alloys · heterogeneous catalysis · hydrogen storage · nanoparticles

[1] a) B. Loges, A. Boddien, F. Gärtner, H. Junge, M. Beller, *Top. Catal.* **2010**, *53*, 902 – 914; b) T. C. Johnson, D. J. Morris, M. Wills, *Chem. Soc. Rev.* **2010**, *39*, 81 – 88; c) S. Enthaler, *ChemSusChem* **2008**, *1*, 801 – 804; d) F. Joó, *ChemSusChem* **2008**, *1*, 805 – 808.

[2] a) A. Boddien, B. Loges, H. Junge, M. Beller, *ChemSusChem* **2008**, *1*, 751 – 758; b) B. Loges, A. Boddien, H. Junge, M. Beller, *Angew. Chem.* **2008**, *120*, 4026 – 4029; *Angew. Chem. Int. Ed.* **2008**, *47*, 3962 – 3965; c) C. Fellay, P. J. Dyson, G. Laurenczy, *Angew. Chem.* **2008**, *120*, 4030 – 4032; *Angew. Chem. Int. Ed.* **2008**, *47*, 3966 – 3968; d) Y. Himeda, *Green Chem.* **2009**, *11*, 2018 – 2022; e) W. Gan, C. Fellay, P. J. Dyson, G. Laurenczy, *J. Coord. Chem.* **2010**, *63*, 2685 – 2694.

[3] M. Grasemann, G. Laurency, *Energy Environ. Sci.* **2012**, *5*, 8171 – 8181.

[4] a) S. W. Ting, S. Cheng, K. Y. Tsang, N. Laak, K. Y. Chan, *Chem. Commun.* **2009**, 7333 – 7335; b) Y. Huang, X. Zhou, M. Yin, C. Liu, W. Xing, *Chem. Mater.* **2010**, *22*, 5122 – 5128.

[5] a) X. Zhou, Y. Huang, W. Xing, C. Liu, J. Liao, T. Lu, *Chem. Commun.* **2008**, 3540 – 3542; b) X. Gu, Z. H. Lu, H. L. Jiang, T. Akita, Q. Xu, *J. Am. Chem. Soc.* **2011**, *133*, 11822 – 11825.

[6] a) D. A. Bulushev, S. Beloshapkin, J. R. H. Ross, *Catal. Today* **2010**, *154*, 7 – 12; b) Q. Y. Bi, X. L. Du, Y. M. Liu, Y. Cao, H. Y. He, K. N. Fan, *J. Am. Chem. Soc.* **2012**, *134*, 8926 – 8933.

[7] N. Akiya, P. E. Savage, *AIChE J.* **1998**, *44*, 405 – 415.

[8] K. Tedsree, T. Li, S. Jones, C. W. A. Chan, K. M. K. Yu, P. A. J. Bagot, E. A. Marquis, G. D. W. Smith, S. C. E. Tsang, *Nat. Nanotechnol.* **2011**, *6*, 302 – 307.

[9] Ö. Metin, X. Sun, S. Sun, *Nanoscale* **2013**, *5*, 910-912.

[10] a) D. A. Slanac, W. G. Hardin, K. P. Johnston, K. J. Stevenson, *J. Am. Chem. Soc.* **2012**, *134*, 9812 – 9819; b) J. Yang, J. Yang, J. Y. Yang, *ACS Nano* **2012**, *6*, 9373 – 9382.

[11] F. Abild-Pedersen, M. P. Andersson, *Surf. Sci.* **2007**, *601*, 1747 – 1753.

[12] V. Mazumder, S. Sun, *J. Am. Chem. Soc.* **2009**, *131*, 4588 – 4589.